Newtonian Poiseuille flows with pressure-dependent wall slip

Pandelitsa Panaseti

Department of Mathematics and Statistics, University of Cyprus, P.O. Box 20537, Nicosia, Cyprus

Kostas D. Housiadas

Department of Mathematics, University of the Aegean, Karlovassi, Samos 83200, Greece

Georgios C. Georgiou[a)]

Department of Mathematics and Statistics, University of Cyprus, P.O. Box 20537, Nicosia, Cyprus

(Received 1 June 2012; final revision received 23 October 2012; published 6 December 2012)

Synopsis

The effect of pressure-dependent slip at the wall in steady, isothermal, incompressible Poiseuille flows of a Newtonian liquid is investigated. Exponential dependence of the slip coefficient on the pressure is assumed and the flow problems are solved using a regular perturbation scheme in terms of the exponential decay parameter of the slip coefficient. The sequence of partial differential equations resulting from the perturbation procedure is solved analytically up to second order. The two-dimensional solution reveals the effects of the slip decay coefficient and the other dimensionless numbers and parameters, in the flow. The average pressure drop and the skin friction factor are also derived and discussed. © *2013 The Society of Rheology*.
[http://dx.doi.org/10.1122/1.4769823]

I. INTRODUCTION

The importance of slip at the wall in viscous flows has been emphasized in many studies during the past few decades. Barnes (1995) reviewed and discussed wall depletion (i.e., slip) of polymer solutions, emulsions, and suspensions in viscometers, while Denn (2001) reviewed theories of slip and the relation between slip and extrusion instabilities. Recent review papers of wall slip cover the literature not only of molten high-molecular-weight polymers [Hatzikiriakos (2012)] but also of Newtonian liquids [Neto *et al.* (2005)]. Neto *et al.* (2005) reviewed experimental studies regarding the phenomenon of slip of Newtonian liquids at solid interfaces, which is of interest in the fields of

[a)]Author to whom correspondence should be addressed; electronic mail: georgios@ucy.ac.cy

microfluidic and microeletromechanical devices. They emphasized in particular the importance of surface roughness, wettability, and gaseous film or nanobubbles at the interface. The violation of the classical no-slip boundary condition becomes more pronounced in the case of non-Newtonian fluids, such as suspensions, emulsions, and polymer melts and solutions, leading to more interesting phenomena and instabilities [Denn (2011)]. Sochi (2011) notes that slip effects become more important in non-Newtonian systems, since they affect the shear rate near the wall and therefore all parameters depending on the latter. Molten polymers are known to slip macroscopically at solid surfaces above a critical wall shear stress [Hatzikiriakos (2012)]. In fact, beyond a second critical wall shear stress, transition from a weak to strong slip takes place [Wang and Drda (1996); Hatzikiriakos (2012)].

Hatzikiriakos (2012) reviewed both static and dynamic slip models and discussed their significance on the rheology and flow simulations of molten polymers. Most static models assume that the slip velocity u_w^*, defined as fluid velocity relative to the wall, depends on the instantaneous value of the wall shear stress, τ_w^*. (In the present work, we use star superscripts to denote dimensional quantities.) A simple slip equation employed by various researchers [Lau and Schowalter (1986); Hill *et al.* (1990); Hatzikiriakos and Dealy (1992); Barnes (1995)] is the power-law expression

$$u_w^* = \alpha^* \tau_w^{*m}, \tag{1}$$

where α^* is the slip coefficient and m is the power-law exponent. The slip coefficient varies in general with temperature, normal stress and pressure, molecular parameters, and the characteristics of the fluid/wall interface. When $m = 1$, the slip coefficient is also defined as the ratio of the extrapolation length (i.e., the characteristic length equal to the distance that the velocity profile at the wall must be extrapolated to reach zero) to the viscosity [Hatzikiriakos (2012)]. The no-slip boundary condition is recovered when $\alpha^* = 0$, whereas perfect slip is achieved when α^* becomes infinite.

Experimental observations also suggest that the slip velocity may also depend on the normal stresses, which include pressure, as well as on the past states of the local wall shear [Hatzikiriakos (2012), and references therein]. In general, the dependence of the slip velocity on the normal stress is weaker than that on the shear stress. The slip coefficient as well as the slip velocity decreases with the normal stress. This implies, for example, that slip is weak or completely suppressed upstream and becomes stronger downstream and near the exit of a tube. Experimental evidence for this phenomenon has been reported by various investigators. The early capillary extrusion experiments of Vinogradov and Ivanova (1968) showed that at elevated pressures melt fracture is suppressed, due presumably to the reduction of slip at high pressures. White *et al.* (1991) tested various elastomeric compounds in a biconical rheometer and found that decreasing the pressure leads to higher slip velocities while high pressures suppress slip. Hatzikiriakos and Dealy (1992) demonstrated that Mooney's technique of calculating slip velocities from capillary dies of different diameters fails either if the viscosity or the slip velocity depends upon the pressure or if there are significant temperature gradients, and proposed a revised technique that accounts for the effects of normal stresses and pressure. Hatzikiriakos and Dealy (1992) proposed a slip equation accounting also for temperature effects in which the slip coefficient is a decreasing function of the wall normal stress. A different slip model has been proposed by Stewart (1993), which involves the dependence of slip on the density.

Hill *et al.* (1990) used the theory of elastomer adhesion and proposed a framework of adhesive failure between the polymer melt and the wall according to which the slip coefficient decays exponentially with the isotropic pressure p^*:

$$\alpha^* = A^* \mathrm{e}^{-\varepsilon^* p^*}, \tag{2}$$

where A^* is the slip coefficient at zero pressure and ε^* is the pressure decay parameter. Equation (2) was later used by Person and Denn (1997) in a study of the flow of a power-law fluid in a channel. The slip equation proposed by Wang *et al.* (2010) includes an additional exponential term accounting for temperature effects. Similarly, Hatzikiriakos and Dealy (1992) formulated a theoretical model based on an extension of analysis of Lau and Schowalter (1986), which, despite its different theoretical basis, was of form similar to that of Eq. (2). However, Hatzikiriakos and Dealy (1992) found a stronger pressure dependence at moderate pressures and saturation at higher pressures.

The effects of the pressure-dependence of slip have also been investigated by means of numerical simulations and/or asymptotic analyses. Kumar and Graham (1998) modified the arbitrary nonmonotonic, pressure-independent slip equation proposed by Georgiou and Crochet (1994) to add pressure-dependent slip in their study of polymer extrusion instabilities. Rao and Rajagopal (1999) solved the Newtonian flow in a channel using three different slip equations in which the slip velocity depended (a) only on the shear stress, (b) only on the normal stress, and (c) on both the shear and the normal stresses. In the latter case, the slip velocity was actually expressed as a function of the ratio of the shear stress to the normal stress. Their finite volume solutions showed that the flow is qualitatively different (that is, two-dimensional) and that the pressure gradient is no longer constant along the channel. Ramos (2007) performed an asymptotic analysis of incompressible flow of a Newtonian fluid in a channel assuming that the slip length depends on the pressure and/or the axial pressure gradient and derived analytical solutions of the leading order equations for several slip lengths. He showed that, in general, the pressure gradient is not constant and depends on both the inlet and the outlet pressures. Tang and Kalyon (2008a, 2008b) also developed a mathematical model describing the time-dependent pressure-driven flow of compressible polymeric liquids subject to pressure-dependent slip. They assumed that the slip coefficient α^* is inversely proportional to the pressure. Tang and Kalyon (2008a) also noted that the main underlying mechanisms for the pressure-dependence of wall slip in the case of polymer suspensions are the entrainment of air into the binder phase and the residence time dependence of the establishment of the apparent slip condition.

Recently, Damianou *et al.* (2013) derived approximate semi-analytical solutions of the steady plane and axisymmetric weakly compressible Poiseuille flows of a Herschel–Bulkley fluid using the lubrication approximation and assuming that the slip coefficient follows either Eq. (2) or decreases linearly with pressure. Under the lubrication approximation, Tang (2012) also derived analytical time-dependent solutions of the same flows. As in Tang and Kalyon (2008a, 2008b), he assumed that $\alpha^* \sim 1/p^*$ and pointed out that such a dependence, also proposed for low-density compressible flow [Bird *et al.* (2002)], is similar to that of Eq. (2).

Here, we investigate the effect of slip at the wall in incompressible Newtonian Poiseuille flows (both planar and axisymmetric) by assuming an exponential type dependence of the slip coefficient on the pressure as in Eq. (2). The technique that we use to solve these flow problems is a regular perturbation procedure according to which the dependent flow variables are expanded as series solutions in terms of the exponential slip coefficient. The perturbation technique, in conjunction with the requirement for a separable solution, leads to two-dimensional expressions for the velocity and the pressure. Such analytical solutions have not been reported before in the literature.

The rest of the paper is organized as follows. In Sec. II, the governing equations accompanied with the suitable boundary and symmetry conditions are presented in both dimensional and dimensionless forms. The perturbation procedure is described in Sec. III and the analytical solution up to second order in terms of the pressure decay parameter is

presented. In Sec. IV, the most important results are presented and discussed. The main conclusions are summarized in Sec. V.

II. GOVERNING EQUATIONS

We consider the isothermal, steady, pressure-driven flow of a Newtonian fluid in two different configurations; a straight channel of length L^* and height $2R^*$ and a circular tube of length L^* and radius R^* (Fig. 1). Hereafter, the auxiliary constant ξ will denote the geometrical configuration; $\xi = 0$ and $\xi = 1$ correspond to the planar and axisymmetric configurations, respectively. For isothermal, steady flow under zero gravity, the conservation equations for mass and momentum are

$$\nabla^* \cdot \mathbf{u}^* = 0, \tag{3}$$

$$\rho^* \mathbf{u}^* \cdot \nabla^* \mathbf{u}^* = -\nabla^* p^* + \eta^* \nabla^{*2} \mathbf{u}^*, \tag{4}$$

where ρ^* is the constant mass density of the fluid, $\mathbf{u}^* = \mathbf{e}_z u_z^* + \mathbf{e}_r u_r^*$ is the velocity vector, with u_z^*, u_r^* being the velocity components along the main- and wall normal directions, respectively, $\mathbf{e}_z, \mathbf{e}_r$ being the unit vectors, and η^* is the constant viscosity.

The system of Eqs. (3) and (4) will be solved over the rectangular flow domain (Fig. 1) with appropriate boundary and auxiliary conditions. We assume that pressure-dependent slip occurs along the wall ($r^* = R^*$) following Eqs. (1) and (2) with $m = 1$. Symmetry conditions are applied along $r^* = 0$, i.e., at the symmetry plane (for the planar configuration) or the axis of symmetry (for the axisymmetric configuration). Also, the pressure is taken as zero at a point of the exit plane ($r^* = R^*, z^* = L^*$), and the volumetric flow rate is specified at the outlet plane ($z^* = L^*$). Hence, the boundary and auxiliary conditions are as follows:

$$u_z^*(R^*, z^*) + A^* \mathrm{e}^{-\varepsilon^* p^*} \eta^* \left(\frac{\partial u_z^*}{\partial r^*} + \frac{\partial u_r^*}{\partial z^*} \right)(R^*, z^*) = 0, \quad 0 \le z^* \le L^*, \tag{5}$$

$$u_r^*(R^*, z^*) = 0, \quad 0 \le z^* \le L^*, \tag{6}$$

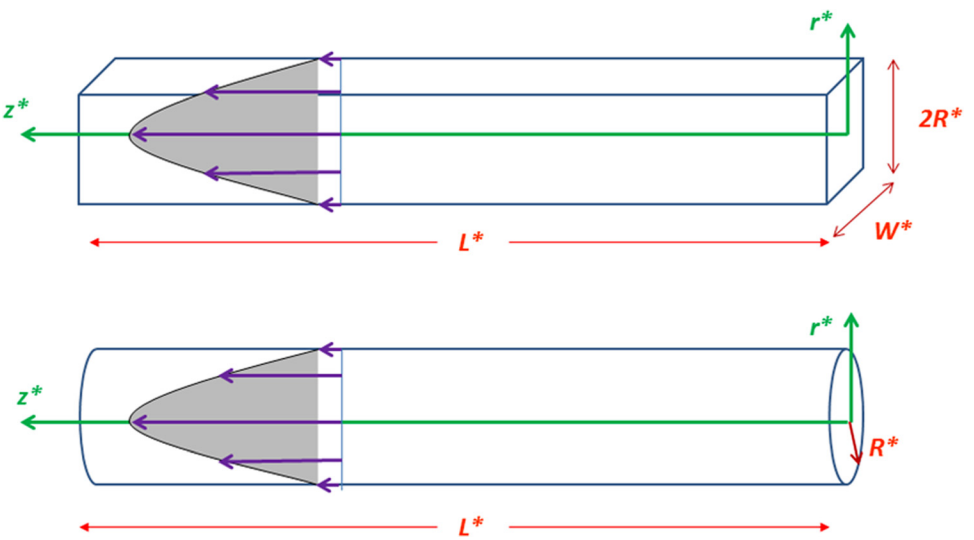

FIG. 1. The geometrical configurations: planar ($\xi = 0$, top) and axisymmetric ($\xi = 1$, bottom).

$$\frac{\partial u_z^*}{\partial r^*}(0,z^*) = u_r^*(0,z^*) = 0, \quad 0 \le z^* \le L^*, \tag{7}$$

$$p^*(R^*,L^*) = 0, \tag{8}$$

$$\int_{S^{*(w)}} u_z^* dS^{*(\xi)} = \dot{Q}^* \quad \text{at } z^* = L^*, \tag{9}$$

where $\dot{Q}^*$ is the constant volumetric flow rate, $dS^{(0)} = W^* dr^*$, W^* being the dimension of the slit in the transverse direction, and $dS^{(1)} = 2\pi r^* dr^*$. No boundary conditions are specified at the inlet plane $(z^* = 0)$, as discussed in previous works on compressible Poiseuille flows [Poinsot and Lele (1992); Venerus (2006); Taliadorou *et al.* (2009); Housiadas and Georgiou (2011); Housiadas *et al.* (2012)].

A. Dimensionless governing equations and auxiliary conditions

Equations (3) and (4) and the auxiliary conditions (5)–(9) are made dimensionless as follows. The axial distance z^* is scaled by L^*, and the wall normal distance r^* by R^*. The axial velocity u_z^* is scaled by the mean velocity

$$U^* \equiv \begin{cases} \dfrac{\dot{Q}^*}{2W^*R^*}, & \xi = 0 \\ \dfrac{\dot{Q}^*}{\pi R^{*2}}, & \xi = 1 \end{cases} \tag{10}$$

and the transverse velocity u_r^* is scaled by U^*R^*/L^*. Finally, the pressure is dedimensionalized using as a scale the characteristic pressure Π^*, defined so that the dimensionless pressure drop along the main flow direction is unity in the case of no slip at the wall:

$$\Pi^* \equiv \begin{cases} \dfrac{3\eta^*\dot{Q}^*L^*}{2W^*R^{*3}}, & \xi = 0 \\ \dfrac{8\eta^*\dot{Q}^*L^*}{\pi R^{*4}}, & \xi = 1 \end{cases}. \tag{11}$$

The dimensionless forms of the continuity equation and the two components of the momentum equation, respectively, are

$$\frac{\partial (r^\xi u_r)}{\partial r} + \frac{\partial (r^\xi u_z)}{\partial z} = 0, \tag{12}$$

$$Re\left(u_r\frac{\partial u_z}{\partial r} + u_z\frac{\partial u_z}{\partial z}\right) = -d^{(\xi)}\frac{\partial p}{\partial z} + c\frac{\partial^2 u_z}{\partial z^2} + \frac{1}{r^\xi}\frac{\partial}{\partial r}\left(r^\xi\frac{\partial u_z}{\partial r}\right), \tag{13}$$

$$cRe\left(u_r\frac{\partial u_r}{\partial r} + u_z\frac{\partial u_r}{\partial z}\right) = -d^{(\xi)}\frac{\partial p}{\partial r} + c^2\frac{\partial^2 u_r}{\partial z^2} + c\frac{\partial}{\partial r}\left\{\frac{1}{r^\xi}\frac{\partial}{\partial r}(r^\xi u_r)\right\}, \tag{14}$$

where $d^{(0)} = 3$ and $d^{(1)} = 8$,

$$Re \equiv \frac{\rho^* U^* R^{*2}}{\eta^* L^*} \tag{15}$$

is the Reynolds number, and

$$c \equiv \left(\frac{R^*}{L^*}\right)^2 \tag{16}$$

is the square of the aspect ratio of the channel or the tube.

The flow domain is $\{-1 \le r \le 1,\ 0 \le z \le 1\}$ and $\{0 \le r \le 1,\ 0 \le z \le 1\}$ for the planar and axisymmetric configurations, respectively. The dimensionless boundary and auxiliary conditions are

$$u_z + A\mathrm{e}^{-\varepsilon p}\left(\frac{\partial u_z}{\partial r} + \frac{\partial u_r}{\partial z}\right) = 0, \quad \text{at } r = 1,\ 0 \le z \le 1, \tag{17}$$

$$u_r = 0, \quad \text{at } r = 1,\ 0 \le z \le 1, \tag{18}$$

$$\frac{\partial u_z}{\partial r} = u_r = 0, \quad \text{at } r = 0, 0 \le z \le 1, \tag{19}$$

$$p = 0 \text{ at } r = z = 1, \tag{20}$$

$$\int_{S^{(\xi)}} u_z dS^{(\xi)} = 1 \quad \text{at } z = 1, \tag{21}$$

where $dS^{(0)} = dr$ and $dS^{(1)} = 2rdr$ for the planar and axisymmetric configurations, respectively. Two additional dimensionless numbers appear in the slip equation (17): The slip number

$$A \equiv \frac{A^*\eta^*}{R^*} \tag{22}$$

and the slip decay coefficient

$$\varepsilon \equiv \varepsilon^*\Pi^*. \tag{23}$$

Obviously, when $A = 0$ the no-slip boundary condition is obtained, whereas when $\varepsilon = 0$ wall slip is pressure-independent and the classical Navier slip condition is recovered.

III. PERTURBATION SOLUTION

A regular perturbation scheme in terms of the slip decay coefficient, ε, is employed up to second order:

$$\left.\begin{aligned} p &= \sum_{j=0}^{2} \frac{p_j \varepsilon^j}{[1 + (3 + \xi)A]^{2j+1}} + O(\varepsilon^3) \\ u_r &= \sum_{j=1}^{2} \frac{u_{r\,j} \varepsilon^j}{[1 + (3 + \xi)A]^{2j+1}} + O(\varepsilon^3) \\ u_z &= \sum_{j=0}^{2} \frac{u_{z\,j} \varepsilon^j}{[1 + (3 + \xi)A]^{2j+1}} + O(\varepsilon^3) \end{aligned}\right\}. \tag{24}$$

Note here that the quantities $[1 + (3 + \xi)A]^{2j+1}$ in the expansions (24) have been introduced only in order to have a more compact solution. Substituting expansions (24) into the governing equations and collecting terms of the same order lead to a sequence of

partial differential equations and accompanying boundary conditions. The zero-, first-, and second-order problems are solved analytically by following a procedure similar to that used by Taliadorou *et al*. (2009), Housiadas and Georgiou (2011), and Poyiadji *et al*. (2012). Details of the derivations are provided in Panaseti (2012).

A. Solution for the planar configuration ($\xi = 0$) up to $O(\varepsilon^2)$

Pressure

$$p = \frac{1-z}{1+3A} + \frac{3\varepsilon A}{2(1+3A)^3}\left\{c(1-r^2) - \frac{6Re(2+7A)}{35(1+3A)^2}(1-z) + (1-z)^2\right\}$$
$$+ \frac{\varepsilon^2 A}{(1+3A)^5}\left\{c\left[\frac{-1-9A+90A^2}{10(1+3A)} + 3\left(\frac{1}{2}-3A\right)r^2\right](1-z) + \left(-\frac{1}{2}+3A\right)(1-z)^3\right.$$
$$+ \frac{Re}{1+3A}\left[\frac{c}{140}\left\{\frac{3(5-54A-315A^2)}{(1+3A)} + \frac{3(-12+61A+399A^2)}{(1+3A)}r^2\right.\right.$$
$$\left.+35(1-3A)r^4 + 7(-2+3A)r^6\right\} + \frac{9(1-8A-42A^2)}{35(1+3A)}(1-z)^2\Bigg]$$
$$\left.+Re^2\left[\frac{156+5690A+27909A^2-12474A^3-166320A^4}{13475(1+3A)^4}(1-z)\right]\right\}. \tag{25}$$

Velocity in the main flow direction

$$u_z = \frac{3(1+2A-r^2)}{2(1+3A)} + \frac{3\varepsilon A}{2(1+3A)^3}\left[(1-3r^2)(1-z) + \frac{Reu_z^{(Re)}}{1+3A}\right]$$
$$+ \frac{\varepsilon^2 A}{(1+3A)^5}\left[u_z^{(Re,0)} + \frac{Re\,u_z^{(Re,1)}}{1+3A} + \frac{Re^2 u_z^{(Re,2)}}{(1+3A)^2}\right], \tag{26a}$$

where

$$u_z^{(Re)} = \frac{5+52A+147A^2}{140(1+3A)} - \frac{3(11+91A+210A^2)}{140(1+3A)}r^2 + \frac{1+3A}{4}r^4 - \frac{1}{20}r^6,$$
$$u_z^{(Re,0)} = \frac{3(1-6A)}{4}\left\{(1-3r^2) + c\left[\frac{3(-1-7A)}{5(1+3A)} + \frac{3(1+5A)}{2(1+3A)}r^2 - r^4\right] - (1-3r^2)(1-z)^2\right\},$$
$$u_z^{(Re,1)} = \frac{3(1-z)}{8}\left\{\begin{array}{l}\dfrac{2(-5-116A-225A^2+882A^3)}{7(1+3A)} + \dfrac{6(11+122A+63A^2-1260A^3)}{7(1+3A)}r^2 \\ +(-1+3A+18A^2)r^4 + \dfrac{1-9A}{5}r^6\end{array}\right\},$$
$$u_z^{(Re,2)} = -\frac{4852+117346A+977871A^2+3001572A^3-979209A^4-15467760A^5}{280(1+3A)^2}$$
$$-\frac{9(-422+1110A+61281A^2+359370A^3)}{140(1+3A)^2}r^2 + \frac{3(-28-250A-63A^2+2520A^3)}{2240}r^4$$
$$+\frac{3(46-264A+525A^2+4725A^3+3780A^4)}{10}r^6 + \frac{9(-4+6A+57A^2)}{4480}r^8 + \frac{5-24A}{5600}r^{10}. \tag{26b}$$

Transverse velocity

$$u_r = \frac{3A\varepsilon\, r(1-r^2)}{2(1+3A)^3}\left\{1-\frac{\varepsilon}{(1+3A)^2}\left[(1-6A)(1-z)+\frac{Re}{140(1+3A)}\right.\right.$$
$$\left.\left.\times\left\{\frac{5+116A+225A^2-882A^3}{1+3A}-6(1-2A-21A^2)r^2+(1-9A)r^4\right\}\right]\right\}. \quad (27)$$

B. Solution for the axisymmetric configuration ($\xi = 1$) up to $O(\varepsilon^2)$

Pressure

$$p = \frac{1-z}{1+4A}+\frac{\varepsilon A}{(1+4A)^3}\left\{c(1-r^2)+2(1-z)^2-\frac{Re}{2(1+4A)}(1-z)\right\}$$
$$+\frac{\varepsilon^2 A}{(1+4A)^5}\left\{\frac{2}{3}(-1+8A)(1-z)^3+\frac{Re}{1+4A}\left(\frac{1}{4}-4A\right)(1-z)^2\right.$$
$$+(1-z)\left[\frac{c(-1-4A+96A^2)}{6(1+4A)}+c(1-8A)r^2+Re^2\frac{33+716A-408A^2-11520A^3}{2160(1+4A)^3}\right]$$
$$\left.+\frac{cARe}{1+4A}\left(\frac{2-39A}{36}+\frac{-1+10A}{8}r^2+\frac{1-2A}{8}r^4+\frac{-2+3A}{36}r^6\right)\right\}. \quad (28)$$

Velocity in the main flow direction

$$u_z = \frac{2(1+2A-r^2)}{1+4A}+\frac{\varepsilon A}{(1+4A)^3}\left\{4(1-2r^2)(1-z)\right.$$
$$\left.+Re\left[\frac{2(1+6A)}{9(1+4\mathrm{A})}-r^2+\frac{1+2A}{1+4A}r^4-\frac{2}{9(1+4A)}r^6\right]\right\}$$
$$+\frac{\varepsilon^2 A}{(1+4A)^5}\left\{u_z^{(Re,0)}+\frac{Re(1-z)}{1+4A}u_z^{(Re,1)}+\frac{Re^2}{(1+4A)^2}u_z^{(Re,2)}\right\}, \quad (29a)$$

where

$$u_z^{(Re,0)} = -2(1-8A)(1+2r^2)(1-z)^2+\frac{c(-1+64A^2)}{3(1+4A)}+\frac{4c(1-2A-48A^2)}{3(1+4A)}r^2-(1-8A)r^4,$$
$$u_z^{(Re,1)} = \frac{2}{9}(-1-9A+48A^2)+(1-32A^2)r^2+(-1+8A+16A^2)r^4+\frac{2}{9}(1-12A)r^6,$$
$$u_z^{(Re,2)} = \frac{-78-1049A-2248A^2+18240A^3+67200A^4}{5400(1+4A)}$$
$$+\frac{87+844A-312A^2-20160A^3-46080A^4}{1080(1+4A)}r^2$$
$$+\frac{-9-10A+336A^2+576A^3}{72}r^4+\frac{3-12A-104A^2-64A^3}{36}r^6$$
$$+\frac{-2+15A+36A^2}{72}r^8+\frac{3-28A}{900}r^{10}. \quad (29b)$$

Transverse velocity

$$u_r = \frac{2\varepsilon A r(1-r^2)}{(1+4A)^3}\left\{1 - \frac{\varepsilon}{(1+4A)^2}\left[2(1-8A)(1-z) - \frac{Re}{36(1+4A)}\{4(1-9A-36A^2) - (5-36A-96A^2)r^2 + (1-12A)r^4\}\right]\right\}. \quad (30)$$

IV. DISCUSSION

We first check the validity of the perturbation scheme. Since the dimensionless slip coefficient $\alpha(p) = A\exp(-\varepsilon p)$ is always positive, this must be hold for the perturbation solution as well, i.e., the reduced slip coefficient is approximated as follows:

$$\exp(-\varepsilon p) \approx 1 - \frac{\varepsilon p_0}{1+(3+\xi)A} + \frac{\varepsilon^2}{[1+(3+\xi)A]^3}\left\{\frac{1+(3+\xi)A}{2}p_0^2 - p_1\right\} > 0. \quad (31)$$

The worst case scenario is for $r = z = 0$ for which inequality (31) gives $\varepsilon < \varepsilon_c$ where

$$\varepsilon_c = \begin{cases} \dfrac{2}{1+3\mathrm{A}+\sqrt{(1+3\mathrm{A})[6A(1+c)-(1+3A)] - \dfrac{36}{35}A(2+7A)Re}}, & \xi = 0 \\ \dfrac{2}{1+4\mathrm{A}+\sqrt{(1+4\mathrm{A})[-(1+4A)+2A(4+2c-Re)]}}, & \xi = 1 \end{cases} \quad (32)$$

is the biggest admissible value of ε. Expression (32) is valid under the requirement that the quantities in the square root are positive; otherwise, inequality (31) is satisfied for any ε.

Given that the flow is assumed to be laminar, the Reynolds number in the planar case (based on the channel height and the average velocity) must be less than 1800, approximately. Similarly, in the axisymmetric case the Reynolds number (based on the pipe diameter and the mean velocity) must be less than 2300. In terms of the Reynolds number as defined in Eq. (15), one finds that it should be $Re \lesssim 900\sqrt{c}$ and $Re \lesssim 1150\sqrt{c}$ for the planar and axisymmetric cases, respectively. The precise upper limit for the Reynolds number requires stability analysis, which however is beyond the scope of the present work.

A. Primary flow variables

Obviously, the zero-order solution is the standard Poiseuille flow solution with Navier (i.e., pressure-independent) wall slip, which is unidirectional; u_z is parabolic, p is linear, and $u_r = 0$. From Eqs. (22) and (25), it is deduced that at first order u_z deviates from the parabolic profile, due to the combined effect of wall slip and inertia. The deviations, $\delta u_z = u_z - u_{z0}$, for $A = 0.05$, $Re = 1$, $\varepsilon = 0.1$, and various axial positions ($z = 0.1$, 0.5, and 0.9) are shown in Fig. 2. For both configurations, the deviation decreases upstream, as expected. The deviation is positive near the entrance and negative near the exit. Changing the slip coefficient A changes the magnitude but the shape of the deviation δu_z remains the same.

As far as the transverse velocity component, u_r, is concerned, Eqs. (27) and (30) reveal that inertia contributes only to second order. Note that the dependence on the Reynolds number is linear. However, the dependence of u_r on the slip coefficient is very

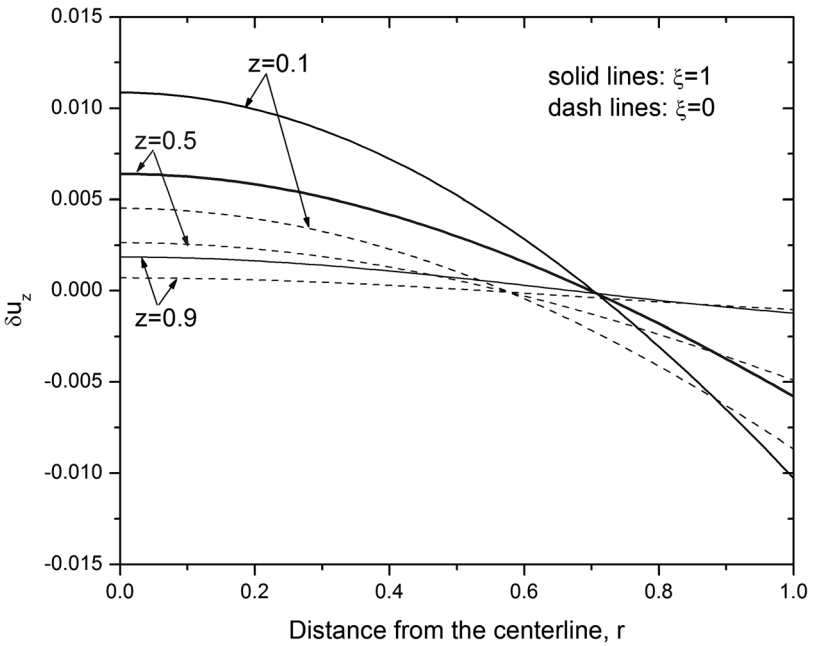

FIG. 2. Deviation from the parabolic velocity profile, $\delta u_z = u_z - u_{z0}$, for $\xi = 0$ (planar configuration) and $\xi = 1$ (axisymmetric configuration); $Re = 1$, $A = 0.05$, $\varepsilon = 0.1$, and $c = 10^{-4}$.

complex. For instance, it is easily shown that $|u_y| \leq \frac{\varepsilon A}{\sqrt{3}(1+3A)^3} + O(\varepsilon^2)$ and $|u_r| \leq \frac{4\varepsilon A}{3\sqrt{3}(1+3A)^3} + O(\varepsilon^2)$ for the planar and axisymmetric configurations, respectively. Note that in both cases the upper bound corresponds to $r = 1/\sqrt{3} \approx 0.577$. The transverse velocity is zero for $A = 0$ (no slip) and increases as A is increased, up to a maximum at $A = 1/6$, and then decreases exponentially; in the limiting case $A \to \infty$, the flow is plug and the transverse velocity tends to zero.

The contours of u_r for the planar configuration, $A = 0.05$, $Re = 1$, $\varepsilon = 0.2$, and $c = 10^{-4}$, are shown in Fig. 3. The transverse velocity vanishes along the symmetry plane ($r = 0$) and along the wall ($r = 1$). It is clear from Eq. (27) that at first order u_r is always positive and reaches a maximum approximately at $r \approx 0.58$. The maximum value increases downstream due to the contribution of the second order. It should be noted that this contribution is positive provided that $A < 1/6$. Hence, the fastest transverse motion of the fluid takes place at the exit plane of the channel.

Fluid motion in the transverse direction and the deviation from parabolic profile are induced by the pressure gradient. At zero order, the dimensionless pressure and its gradient depend only on the slip number A. However, a first order slip effects are combined with those of inertia. It is interesting to note that the derivative $\partial p/\partial r$ is independent of the Reynolds number. In Fig. 4, we compare the pressure contours obtained with $Re = 1$ and $c = 10^{-4}$ in the case of no slip ($A = 0$, dotted lines) with those obtained in the case of pressure-dependent slip with $A = 0.05$ and $\varepsilon = 0.2$. The effect of the slip coefficient is significant; although the contours are similar, almost vertical and equidistant, they are shifted toward the entrance of the channel in the case of slip. This is of course expected given that the pressure gradient is reduced downstream due to slip. It is easily deduced from Eq. (28) that at zero order the pressure is independent of r and varies linearly z. Moreover, the cross-section averaged pressure varies quadratically with z at first order and cubically at second order.

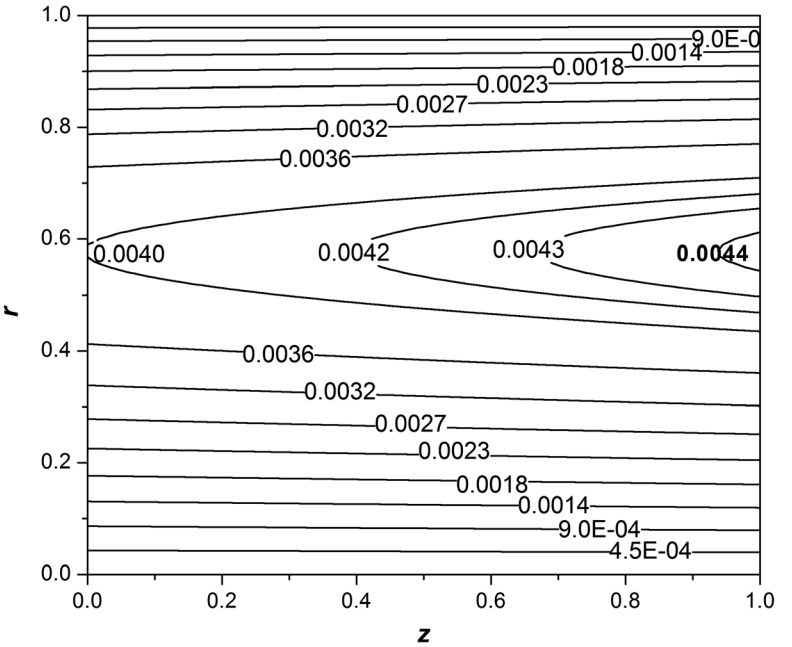

FIG. 3. Contours of the transverse velocity in plane Poiseuille flow; $Re = 1$, $A = 0.05$, $\varepsilon = 0.2$, and $c = 10^{-4}$.

Damianou *et al.* (2013) employed the lubrication approximation [i.e., they assumed that $u_r = 0$ and $p = p(z)$] to derive approximations of the pressure and the axial velocity in the case of the axisymmetric Poiseuille flow with pressure-dependent slip, such that

$$\alpha(p) = A(1 - \varepsilon p). \tag{33}$$

With the notation of the present work, the lubrication solution reads

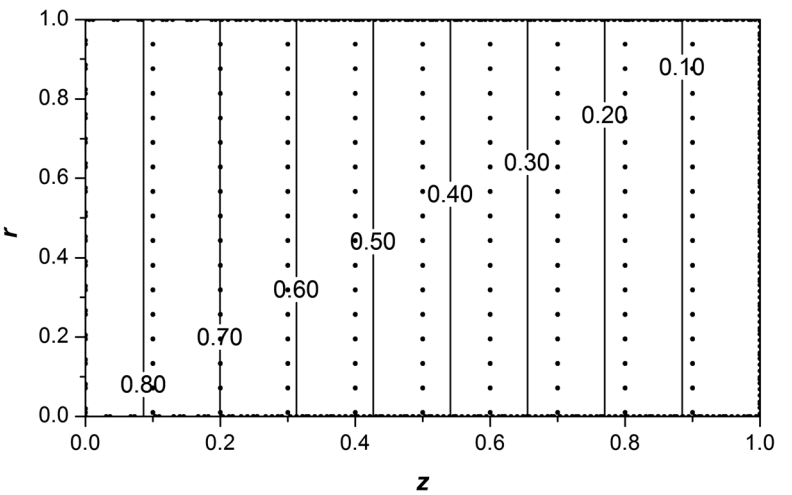

FIG. 4. Pressure contours for the planar configuration for $A = 0$ (no slip, dotted lines) and $A = 0.05$ with $\varepsilon = 0.2$ (solid lines); $Re = 1$ and $c = 10^{-4}$.

$$p(z) = \frac{1+4A}{4\varepsilon A}\left[1 - \sqrt{1 - \frac{8\varepsilon A(1-z)}{(1+4A)^2}}\right] \tag{34}$$

and

$$u_z(r,z) = 1 + \frac{1-2r^2}{(1+4A)\sqrt{1 - \frac{8\varepsilon A(1-z)}{(1+4A)^2}}}. \tag{35}$$

It is easily shown that Eqs. (34) and (35) coincide up to first order with Eqs. (28) and (29), respectively, only when $Re = 0$ and $c = 0$, i.e., when the basic conditions of the lubrication approximation are satisfied.

In Fig. 5, we plotted the reduced slip coefficient, $\exp(-\varepsilon p)$, calculated along the wall for $Re = 1$, $c = 10^{-4}$, $\varepsilon = 0.1$, and various slip numbers. It is interesting to note that the pressure-dependence effect is more pronounced in the case of weak slip, since the pressure required to drive the flow is higher. Another interesting feature of the reduced slip coefficient is that, up to $O(\varepsilon^2)$, does not depend on the square of the aspect ratio, c. The effect of the slip decay parameter ε on the slip velocity $u_w(z) = u_z(1,z)$ is illustrated in Fig. 6, where we show results for the planar flow with $A = 0.1$, $c = 10^{-4}$, and $Re = 1$. For this choice of parameters, the distribution of the slip velocity is almost linear and its slope increases with the slip decay parameter.

B. Pressure drop and friction factor

We use the symbol Δ to denote the difference of a quantity $\phi(r,z)$ between the inlet and the outlet planes, i.e., $\Delta\phi \equiv \phi(r,0) - \phi(r,1)$. We also define the average of a

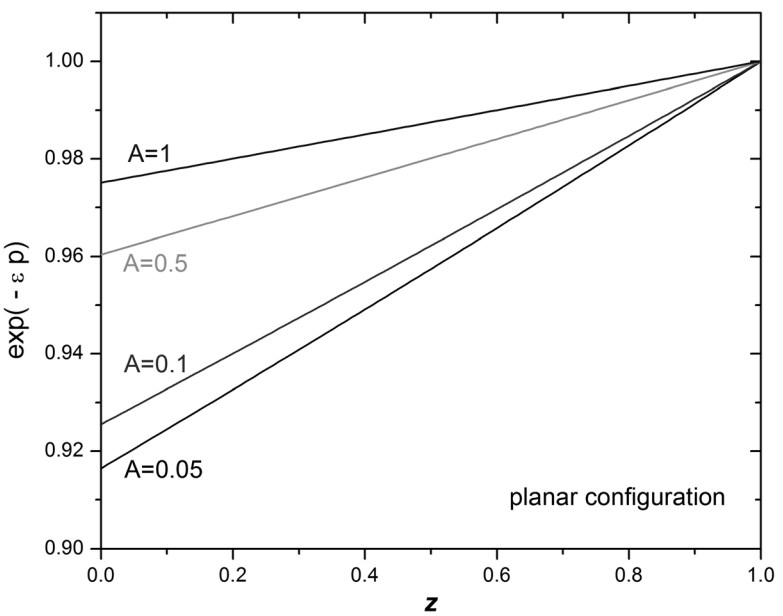

FIG. 5. The reduced slip coefficient across the channel (planar configuration) for various slip coefficients A, $\varepsilon = 0.1$, $Re = 1$, and $c = 10^{-4}$.

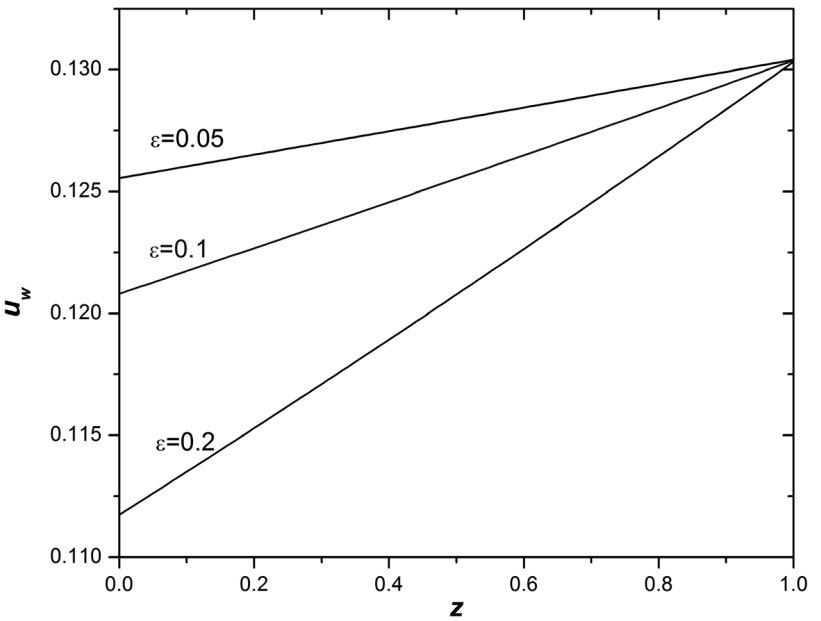

FIG. 6. Slip velocity in plane Poiseuille flow (planar configuration) for different values of the slip decay coefficient when $A = 0.05$, $Re = 1$, and $c = 10^{-4}$.

variable ϕ at a cross section of the channel or circular tube by $\langle\phi\rangle \equiv (1+\xi)\int_0^1 r^{\xi}\phi dr$. Then, by virtue of Eq. (25), the average pressure drop for the planar case, up to $O(\varepsilon^2)$, is given by

$$\Delta\langle p\rangle = \frac{1}{1+3A} + \frac{3A\varepsilon}{2(1+3A)^3}\left[1 - \frac{6(2+7A)}{35(1+3A)^2}Re\right] + \frac{\varepsilon^2 A}{(1+3A)^6}\left\{\frac{(-1+6A)[5(1+3A)-4c]}{10} + \frac{9(1-8A-42A^2)}{35(1+3A)}Re + \frac{156+3A(5690/3+9303A-4158A^2-55440A^3)}{13475(1+3A)^3}Re^2\right\}. \quad (36)$$

Similarly, by means of Eq. (28), one gets the corresponding expression for the axisymmetric case:

$$\Delta\langle p\rangle = \frac{1}{1+4A} + \frac{2\varepsilon A}{(1+4A)^3}\left(1 - \frac{1}{4(1+4A)}Re\right) + \frac{\varepsilon^2 A}{(1+4A)^6}\left[\frac{(-1+8A)(2+8A-c)}{3} + \frac{1-16A}{4}Re + \frac{33+4A(179-102A-2880A^2)}{2160(1+4A)^2}Re^2\right]. \quad (37)$$

Equations (36) and (37) are generalizations of the corresponding dimensionless Hagen–Poiseuille formulas in the case of pressure-dependent slip.

Another quantity of interest is the friction factor, which actually represents a dimensionless shear stress at the wall. The Darcy friction factor, f, is defined as follows:

$$f \equiv -4\eta^* \left(\frac{\partial u_z^*}{\partial r^*}\right)_{r=R^*} \Big/ \left(\frac{1}{2}\rho^* U^{*2}\right). \tag{38}$$

Using the characteristic scales mentioned in Sec. II, the dimensionless average Darcy friction factor, $\bar{f}$, along the entire tube, results from the integration of Eq. (38) from the entrance ($z=0$) to the exit ($z=1$) of the tube. In addition, by using the solution for the velocity in the main flow direction, we find that at second order

$$\begin{aligned}\frac{Re}{24\sqrt{c}}\bar{f} = {} & \frac{1}{1+3A} + \frac{3\varepsilon A}{2(1+3A)^3}\left[1 - \frac{2(4+21A)}{105(1+3A)^2}Re\right] \\ & + \frac{\varepsilon^2 A}{(1+3A)^6}\left\{\frac{(-1+6A)[5(1+3A)-4c]}{10} + \frac{2-30A-189A^2}{35(1+3A)}Re\right. \\ & \left. + \frac{160+3A(1378+8967A+8316A^2-41580A^3)}{40425(1+3A)^3}Re^2\right\}\end{aligned} \tag{39}$$

for the planar case and

$$\begin{aligned}\frac{Re}{32\sqrt{c}}\bar{f} = {} & \frac{1}{1+4A} + \frac{2\varepsilon A}{(1+4A)^3}\left(1 - \frac{1}{12(1+4A)}Re\right) \\ & + \frac{\varepsilon^2 A}{(1+4A)^6}\left[\frac{(-1+8A)(2+8A-c)}{3} + \frac{1-24A}{12}Re\right. \\ & \left. + \frac{15+4A(53+6A-720A^2)}{2160(1+4A)^2}Re^2\right]\end{aligned} \tag{40}$$

for the axisymmetric case. Expressions (39) and (40) can also be derived with the aid of the momentum balance in the flow direction. Multiplying Eq. (13) by $(2r)^\xi$, integrating with respect to r, simplifying the result by means of the continuity equation (12), and using the definition of the Darcy friction factor [Eq. (38)], one gets an ordinary differential equation which can be integrated from $z=0$ to 1 to give

$$\frac{Re}{(24+8\xi)\sqrt{c}}\bar{f} = \Delta\langle p\rangle + \frac{Re}{d^{(\xi)}}\Delta\langle u_z^2\rangle. \tag{41}$$

In Eq. (41), it has been taken into account that $\langle u_z\rangle = 1$ which gives $d\langle u_z\rangle/dz = 0$, given that the flow is incompressible. It is worth noting that Eq. (41) is exact, i.e., no approximation or assumptions have been made for its derivation. It is actually a balance between the skin friction factor (dimensionless viscous forces), the pressure drop, and the difference of the average Reynolds stress between the inlet and the outlet planes. In Fig. 7(a), we plot the quantities $(1+3A)\Delta\langle p\rangle$ and $Re(1+3A)\bar{f}/24\sqrt{c}$ for the planar case as functions of the Reynolds number for $A=0.05$ (solid lines) and $A=1$ (dash lines), $\varepsilon = 0.1$, and $c = 10^{-4}$. Similarly, in Fig. 7(b) we plot the corresponding quantities for the axisymmetric case, i.e., $(1+4A)\Delta\langle p\rangle$ and $Re(1+4A)\bar{f}/32\sqrt{c}$. In both configurations, the pressure drop and the Darcy friction factor decrease with the Reynolds number after an initial plateau. It is also clear that the difference between these quantities also increases, which can also directly be deduced from Eq. (41). This difference is due to fluid inertia, as Eqs. (37) and (41) show. Regarding the effect of the constant slip coefficient A, on

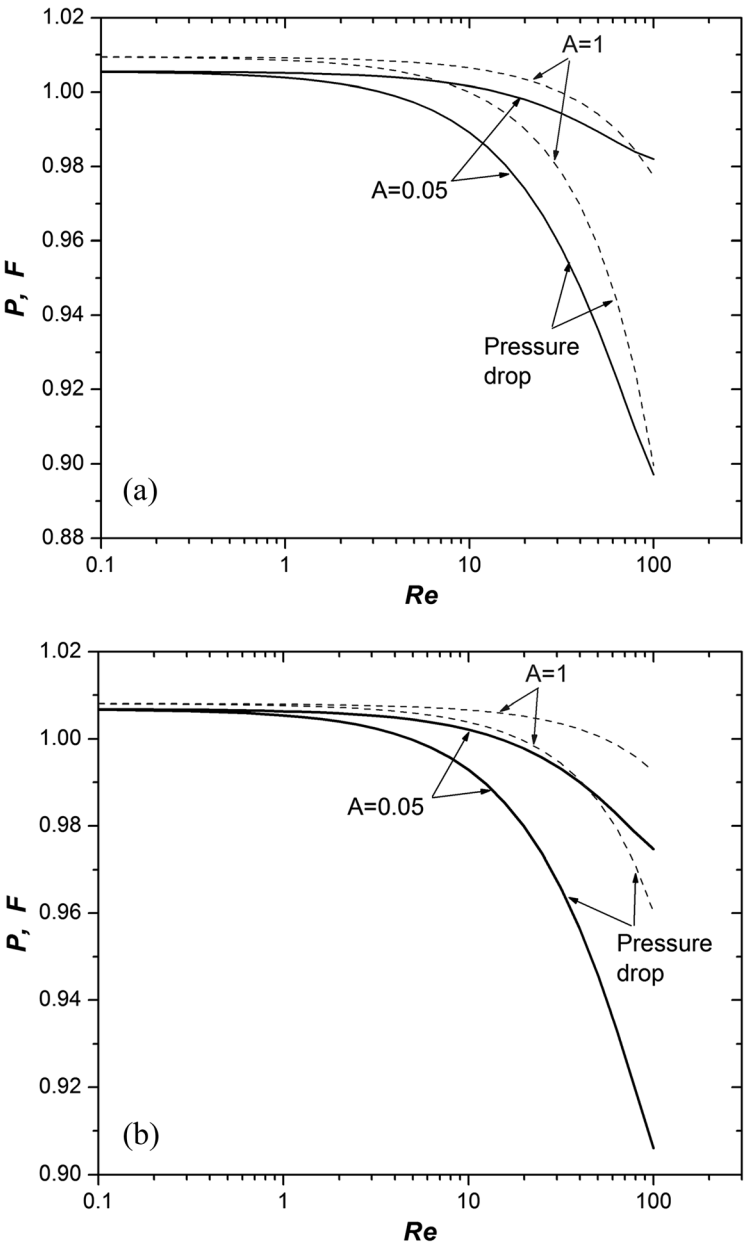

FIG. 7. The Darcy friction factor, $F \equiv Re[1 + (3 + \xi)A]\bar{f}/[(24 + 8\xi)\sqrt{c}]$, and the average pressure drop, $P \equiv (1 + (3 + \xi)A)\Delta\langle p\rangle$, as functions of the Reynolds number, Re: (a) planar configuration; (b) axisymmetric configuration. The solid lines correspond to $A = 0.05$ and the dashed lines to $A = 1$, $\varepsilon = 0.1$, and $c = 10^{-4}$.

$$P \equiv [1 + (3 + \xi)A]\Delta\langle p\rangle \tag{42}$$

and

$$F \equiv \frac{Re[1 + (3 + \xi)A]}{(24 + 8\xi)\sqrt{c}}\bar{f} \tag{43}$$

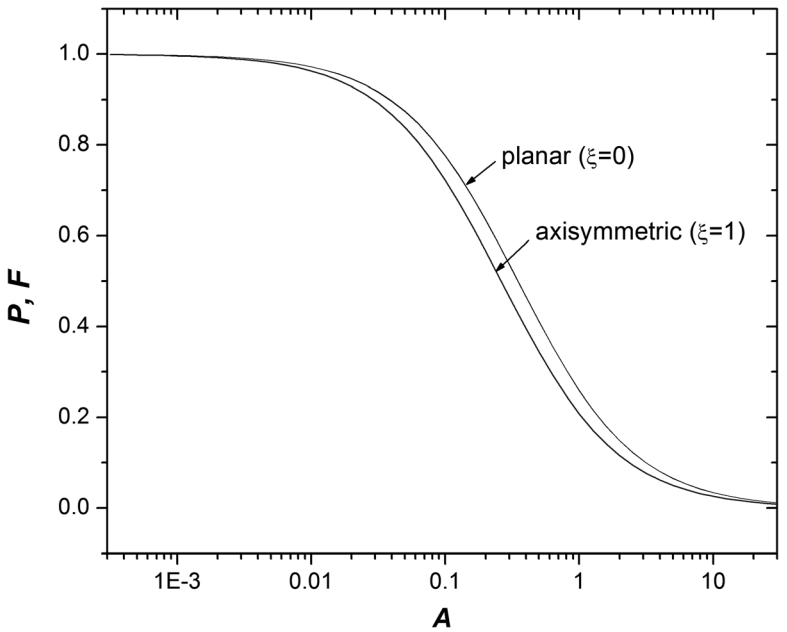

FIG. 8. The Darcy friction factor, $F \equiv Re[1 + (3 + \xi)A]\bar{f}/[(24 + 8\xi)\sqrt{c}]$, and the average pressure drop, $P \equiv [1 + (3 + \xi)A]\Delta\langle p\rangle$, as functions of the slip coefficient, A, when $\varepsilon = 0.1$, $Re = 1$, and $c = 10^{-4}$.

this is not monotonic. As the slip coefficient, A, increases, for constant Reynolds number, P and F decrease. However, a further decrease on A results in an increase for both P and F. Finally, as A goes to zero, P and F go to unity (as they should).

In Fig. 8, we plotted the quantities P and F as functions of the slip coefficient A, for both the planar and the axisymmetric configurations, with $\varepsilon = 0.1$, $Re = 1$, and $c = 10^{-4}$. In contrast to Fig. 7, the pressure drop and the friction factor are practically indistinguishable (for both configurations). As usual, the pressure drop and the friction factor are lower in the axisymmetric case. They decrease in a sigmoidal fashion as A increases; for A less than approximately 0.01, both quantities are close to unity, in the region $0.01 < A < 10$ they decrease substantially, and for $A > 10$ they approach zero asymptotically. It should also be noted that the effect of the square of the aspect ratio, c, is very small; it affects the solution only at second order, which is also seen from Eqs. (36), (37), (39), and (40). The Reynolds number affects the solution at first order but its net effect is very small due to the fact that the slip number A quickly dominates all other contributions.

V. CONCLUSIONS

Perturbation solutions for the laminar, isothermal, incompressible planar and axisymmetric Poiseuille flows of a Newtonian liquid with an exponential dependence of the slip coefficient on the pressure have been derived. The velocity vector and the pressure were expanded as power series of the exponential slip coefficient and the solution was obtained up to second order. Expressions for the pressure drop and the friction factor have been obtained. The derived solution shows that as the constant slip coefficient increases, the effect of the pressure becomes progressively weaker and the slip velocity at the wall becomes more uniform throughout the channel or tube. The analytical solution derived here may be useful in capillary rheometry and for validating numerical algorithms for

flows with pressure-dependent wall slip. In the former case, a modified Mooney technique should be applied using capillaries of different lengths and diameters.

References

Barnes, H. A., "A review of the slip (wall depletion) of polymer solutions, emulsions and particle suspensions in viscometers: Its cause, character, and cure," J. Non-Newtonian Fluid Mech. **56**, 221–251 (1995).

Bird, R. B., W. E. Stewart, and E. N. Lightfoot, *Transport Phenomena*, 2nd ed. (Wiley, New York, 2002).

Damianou, Y., G. C. Georgiou, and I. Moulitsas, "Combined effects of compressibility and slip in flows of a Herschel-Bulkley fluid," J. Non-Newtonian Fluid Mech. (2013).

Denn, M. M., "Extrusion instabilities and wall slip," Annu. Rev. Fluid Mech. **33**, 265–287 (2001).

Georgiou, G. C., and M. J. Crochet, "Compressible viscous flow in slits with slip at the wall," J. Rheol. **38**, 639–654 (1994).

Hatzikiriakos, S. G., "Wall slip of molten polymers," Prog. Polym. Sci. **37**, 624–643 (2012).

Hatzikiriakos, S. G., and J. M. Dealy, "Wall slip of molten high density polyethylenes. II. Capillary rheometer studies," J. Rheol. **36**, 703–741 (1992).

Hill, D. A., T. Hasegawa, and M. M. Denn, "On the apparent relation between the adhesive failure and melt fracture," J. Rheol. **34**, 891–918 (1990).

Housiadas, K. D., and G. C. Georgiou, "Perturbation solution of a weakly compressible Oldroyd-B fluid," J. Non-Newtonian Fluid Mech. **166**, 73–92 (2011).

Housiadas, K. D., G. C. Georgiou, and I. G. Mamoutos, "Laminar axisymmetric flow of a weakly compressible viscoelastic fluid," Rheol. Acta **51**, 511–526 (2012).

Kumar, K. A., and D. Graham, "Effect of pressure-dependent slip on flow curve multiplicity," Rheol. Acta **37**, 245–255 (1998).

Lau, H. C., and W. R. Schowalter, "A model of adhesive failure of viscoelastic fluids during flow," J. Rheol. **30**, 193–206 (1986).

Neto, C., D. R. Evans, E. Bonaccurso, H.-J. Butt, and V. S. J. Graig, "Boundary slip in Newtonian liquids: A review of experimental studies," Rep. Prog. Phys. **68**, 2859–2897 (2005).

Panaseti, P., M.Sc. thesis, University of Cyprus, Nicosia, 2012.

Person, T. J., and M. M. Denn, "The effect of die materials and pressure-dependent slip on the extrusion of linear low-density polyethylene," J. Rheol. **41**, 249–265 (1997).

Poinsot, T., and S. Lele, "Boundary conditions for direct simulations of compressible viscous flows," J. Comput. Phys. **101**, 104–129 (1992).

Poyiadji, S., G. C. Georgiou, K. Kaouri, and K. D. Housiadas, "Perturbation solutions of weakly compressible Newtonian Poiseuille flows with Navier slip at the wall," Rheol. Acta **51**, 497–510 (2012).

Ramos, J. I., "Asymptotic analysis of channel flows with slip lengths that depend on the pressure," Appl. Math. Comput. **188**, 1310–1318 (2007).

Rao, I. J., and K. J. Rajagopal, "The effect of the slip boundary condition on the flow of fluids in a channel," Acta Mech. **135**, 113–126 (1999).

Sochi, T., "Slip at fluid-solid interface," Polym. Rev. **51**, 309–340 (2011).

Stewart, C. W., "Wall slip in the extrusion of linear polyolefins," J. Rheol. **37**, 499–513 (1993).

Taliadorou, E. G., M. Neophytou, and G. C. Georgiou, "Perturbation solutions of Poiseuille flows of weakly compressible Newtonian liquids," J. Non-Newtonian Fluid Mech. **163**, 25–34 (2009).

Tang, H., "Analysis on creeping channel flows of compressible fluids subject to wall slip," Rheol. Acta **51**, 421–439 (2012).

Tang, H. S., and D. M. Kalyon, "Time-dependent tube flow of compressible suspensions subject to pressure-dependent wall slip: Ramifications on development of flow instabilities," J. Rheol. **52**, 1069–1090 (2008a).

Tang, H. S., and D. M. Kalyon, "Unsteady circular tube flow of compressible polymeric liquids subject to pressure-dependent wall slip," J. Rheol. **52**, 507–525 (2008b).

Venerus, D. C., "Laminar capillary flow of compressible viscous fluids," J. Fluid Mech. **555**, 59–80 (2006).

Vinogradov, G. V., and L. L. Ivanova, "Wall slippage and elastic turbulence of polymers in the rubbery state," Rheol. Acta **7**, 243–254 (1968).

Wang, S.-Q., and P. A. Drda, "Stick-slip transition in capillary flow of polyethylene. 2. Molecular weight dependence and low-temperature anomaly," Macromolecules **29**, 4115–4119 (1996).

Wang, Z. Y., Y. C. Lam, X. Chen, and S. C. Joshi, "Viscosity corrections for concentrated suspension in capillary flow with wall slip," AIChE J. **56**, 1447–1455 (2010).

White, J. L., M. H. Han, N. Nakajima, and R. Brzoskowski, "The influence of materials of construction on biconical rotor and capillary measurements of shear viscosity of rubber and its compounds and considerations of slippage," J. Rheol. **35**, 167–189 (1991).